Islamic Azad University

Journal of

Optoelectronical Nanostructures

Summer 2023 / Vol. 8, No. 3

Research Paper (Pape Type)

Design and Modeling of a D–Shaped PCF Refractive Index Sensor Based on SPR Effect

Amin Sayyad Tondro[1], Mojtaba Sadeghi[*,2] , Abbas Kamaly[1], Zahra Adelpour[2], Seyyed Ali Emamghorashi[1]

[1] Department of Electrical Engineering, Fasa Branch, Islamic Azad University, Fasa, Iran

[2] Department of Electrical Engineering, Shiraz Branch, Islamic Azad University, Shiraz, Iran

Received:2 Jul. 2023
Revised: 14 Aug. 2023
Accepted: 20 Aug. 2023
Published:15 Sep. 2023

Use your device to scan and read the article online

Keywords:
PCR, REFRACTIVE INDEX, SENSOR, SPR, SENSITIVITY

Abstract:
This study introduces an efficient D-shaped sensor for refractive index (RI) sensing based on the surface plasmon resonance (SPR) phenomenon. The sensor design was examined through numerical simulations utilizing the finite element method (FEM). The calculations revealed that the proposed fiber demonstrates particular suitability for sensing within the wavelength spectrum spanning from 0.5 to 0.7µm. Our results yielded a remarkable wavelength sensitivity and substantial RI resolution of 9500 nm/RIU and 6.5 $\times 10^{-6}$ RIU, respectively which observed as the analyte RI ranged 1.33~1.36. Additionally, a maximum amplitude sensitivity of 215 RIU^{-1}, accompanied by an impressive linearity of 0.99862 was acheived.

Citation: Amin Sayyad Tondro, Mojtaba Sadeghi, Abbas Kamaly, Zahra Adelpour, Seyyed Ali Emamghorashi. Design and modeling of a D-shaped PCF refractive index sensor based on SPR effect. . **Journal of Optoelectronical Nanostructures.** 2023; 8 (3): 67- 78 **DOI: 10.30495/JOPN.2023.31381.1278**

***Corresponding author:** Mojtaba Sadeghi
Address: Department of Electrical Engineering, Fasa Branch, Islamic Azad University, Fasa, Iran. **Tell:** 00989177916865 **Email:** sadeghi@shiraziau.ac.ir

1. INTRODUCTION

Surface plasmon resonance (SPR) sensors find utility across diverse detection domains owing to their exceptional sensitivity and straightforward operational characteristics. Plasma waves represent collective electron oscillations occurring within the conduction band of two materials at the interface, resonating coherently with the incident field. Surface plasmon resonance can be induced along metal-dielectric interfaces and also through noble metal nanoparticles. Photonic crystal fiber (PCF) presents a promising avenue and has the potential to serve as a highly effective sensing foundation [1-4]. When integrated with the SPR phenomenon, a PCF-based sensor benefits from its compact dimensions and versatile design capabilities, resulting in enhanced sensing characteristics. Wu et al. introduced an ultrahigh-sensitive SPR-PCF and explored the effects of air holes diameter and thickness of gold layer in their work [2]. Based on the structural characteristics of the PCF utilized for light transmission control, a wide array of optical attributes within PCFs – including effective mode area, dispersion, nonlinearity and birefringence of mode – can be effectively manipulated. Sequentially, this manipulation can significantly enhance sensing capabilities. In recent times, there has been a growing focus on the fabrication and examination of D-shaped PCF sensors, driven by the SPR effect. Soroosh et al. introduced a polarization-insensitive for temperature sensing with PCF structure[5]. They employed the FEM to analyze the coupling between the defected clad and core. The numerical simulations revealed that when phase matching between super modes was achieved, peak confinement loss and resonance occurred. In an alternative endeavor, a D-shaped PCF-SPR sensor was introduced, showcasing high sensitivity around 7500 nm/RIU and 1.30×10^{-5} RIU resolution while the refractive index changes between 1.43–1.46 [6]. Ren et al. proposed a RI-SPR sensor using PCF. They explored the sensing characteristics of this sensor through finite element simulations. The proposed sensor offers the capability for dual-waveband measurements. By manipulating the height of the analytes and the wavelength of the light, the sensor exhibited distinct performances [7].

To enable SPR sensing within PCFs, a common approach involves coating the inner PCF holes walls with a thin metal film and subsequently filling the appropriate analyte. The SPR spectrum, responsive to variations in the RI of the surrounded medium at the interface of metal, can be utilized to check changes in this environment. Notably, PCF–SPR sensors often feature air hole diameters in the order of a few microns. Consequently, practical implementation of metal deposition within these holes presents significant challenges. Additionally, in RI PCF–SPR devices, the resulting changes in the spectrum are influenced by the

RI of the medium encircling the metal. Distinguishing between the factors—whether alterations arise from the analyte's RI or temperature—is intricate when assessing the SPR spectrum. As such, achieving effective RI sensing within a PCF–based SPR sensor is inherently demanding. To address these complexities associated with metal coating, one potential solution involves the utilization of D-type or exposed-core PCFs.

In this study, we focused on the visible and near-infrared (NIR) bands to develop and simulate a novel and straightforward D-shaped PCF–SPR sensor. Our investigation aimed to understand the effect of various parameters on sensitivity. Given the considerations of chemical stability and excitation material's resonance output energy, silver (Ag) was chosen as the medium for the sensing layer. We utilized FEM to assess the impact of these variables on the sensing performance of the simulated structure. Additionally, we explored sensor's sensitivity to variations in analyte RI. The introduction of a silver layer on top, alongside the optimization of final design parameters, led to improved overall characteristics in comparison to previously reported outcomes.

2. Model and Analysis

Fig. 1 depicts the cross-sectional view of the proposed sensor structure. Λ=4 µm is the lattice pitch, and the diameters of the air holes are set to d_1 = 3.2 µm and d_2= 1.6 µm. The Ag layer thickness (T_{Ag}) is fixed at 40 nm. Fused silica is used for the PCF material. To explore the properties of PCF-SPR and its sensing capabilities, we have utilized FEM. The RI of fused silica is extracted from the Sellmeier equation as [8]:

$$n(\lambda)=\sqrt{\varepsilon+\frac{A}{\lambda^2}+\frac{B\lambda_1^2}{\lambda^2-\lambda_1^2}} \tag{1}$$

Here, λ is the free space wavelength, the values are as follows: A = 0.939816 µm², and B = 8.10461×10^{-3}, ε = 11.6858, λ_1 = 1.1071 µm. The parameters of Ag is calculated through the L4 model [9].

$$\varepsilon(\omega)=\varepsilon_\infty+\frac{\sigma/\varepsilon_0}{i\omega}+\sum_{p=1}^{4}\frac{C_p}{\omega^2+A_p\omega+B_p} \tag{2}$$

the parameters of this Eq. are taken according to Ref [7].

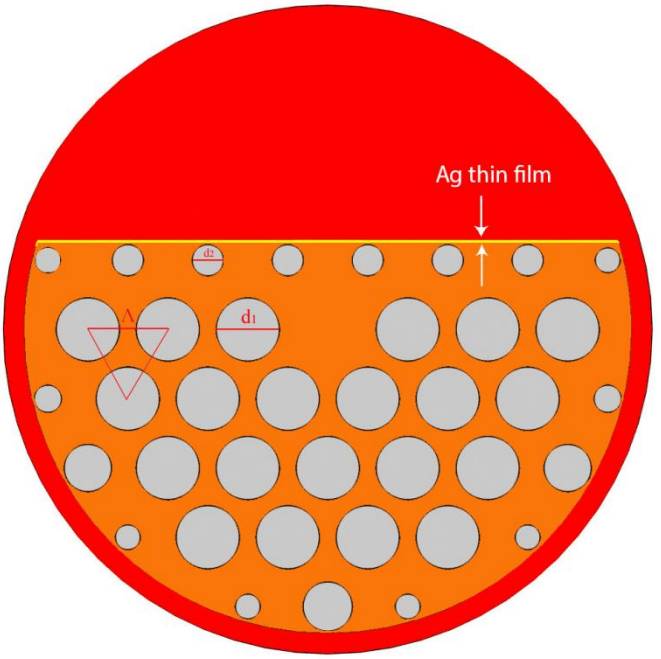

Fig.1. schematic of the proposed PCF-SPR sensor.

Modes will experience coupling when their effective refractive indices (n_{eff}) become equal. For investigation of the coupling performance of the sensor, the E-field distributions, n_{eff} curve and the loss spectra of the modes are shown in Fig. 2. According to the following Eq., the confinement loss is calculated [9]:

$$\alpha_{Loss}(dB/cm) = 8.686 \times \left(\frac{2\pi}{\lambda}\right) \times \mathrm{Im}\left(n_{eff}\right) \times 10^{4} \quad (3)$$

The sensor sensitivity is calculated as [10]:

$$S_n\left(\mu m/RIU\right) = \frac{\Delta\lambda_{peak}}{\Delta n_{Anl.}} \quad (4)$$

where $\Delta\lambda_{peak}$ is the resonance peak shift.

Given that no manipulation is necessary, opting for the amplitude interrogation technique (AIT) becomes a more cost-effective approach to assess the sensor's performance. The sensitivity can be computed by [11]:

$$S_{Amp.}\left(RIU^{-1}\right)=-\frac{1}{\alpha\left(\lambda,n_{Anl.}\right)}\times\frac{\Delta\alpha\left(\lambda,n_{Anl.}\right)}{\Delta n_{Anl.}} \quad (5)$$

where α, $\Delta\alpha$ and $\Delta n_{Anl.}$ are loss, loss difference and changes of the analyte RI, respectively.

During the simulation, the impedance boundary condition is taken into account, and FEM is used for the investigation of the PCF–SPR properties. The sensor is partitioned into triangular subdomains within the FEM framework. The solution of Maxwell's equations using FEM is facilitated by these adjacent subdomains. Furthermore, the effective index and mode field pattern are obtained with greater accuracy through the application of FEM. The simulation involves the utilization of a total of 26,220 domain elements and 1,759 boundary elements.

3. Result and Discussion

In the analyzed sensor, we examined three different modes; (1) the x-polarization core fundamental mode, (2) the y-polarization core FM, and (3) the SPP mode, as illustrated in the inset of Fig. 2. The simulation shows that both of the polarization coexist at the interface. However, only the x-polarization FM can excite surface plasmons. According to Fig.2, when phase matching occurs, a noticeable loss at the intersection happens. Under mode-resonance conditions, the decaying field within the structure intensifies significantly, resulting in a pronounced loss signal. The x-polarization mode resonates solely with the SPP at a wavelength of λ = 500 nm. As a result, just a single loss wave emerges at the intersection point of two curves, offering a highly acceptable configuration for sensing applications. Thanks to distinctiveness of the resonance peak, detection of the analyte's RI is achievable.

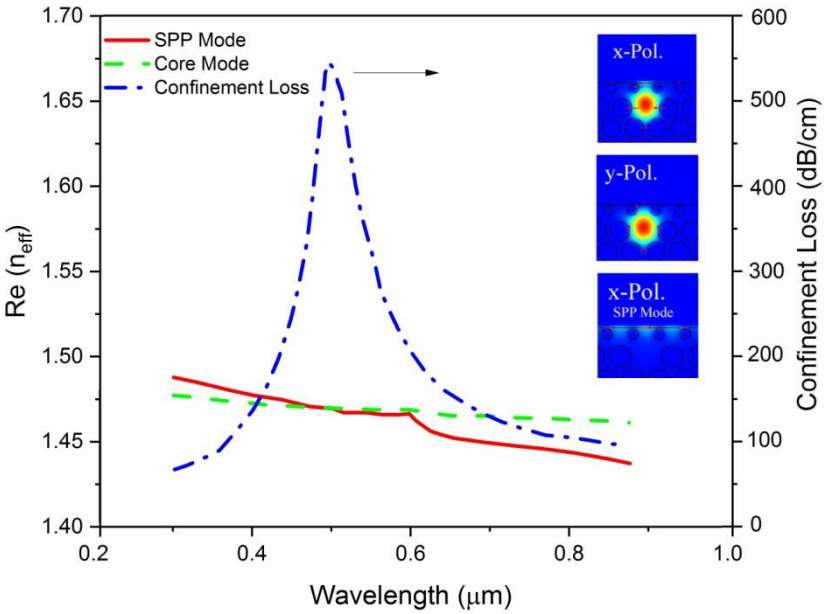

Fig. 2. Real part of RI as the wavelength for SPP and core mode (nAnl.=1.33) and the confinement loss value . Mode patterns of different polarization are shown in the inset.

At the next step, we investigate the influence of various PCF parameters on the sensing characteristics of the sensor. Fig. 3a presents the loss corresponding to different d_1 values, with n_{Anl} =1.33. Evidently, as the d_1 is increased, a red-shift is observed in the resonance peak. Additionally, variations in the intensity of the resonance signal are observable; notably, for d_1 = 4.2 µm, the signal's sharpness diminishes and broadens. This behavior aligns with the reduction in the core area, which impacts the maintenance of optimal single-mode transmission in the PCF. Consequently, there is no strong coupling between the x-polarization FM and the SPP mode. For d_1 = 2.2 and 3.2 µm, the generated energy by the 3.2 µm value surpasses that of the former slightly. Increased loss energy facilitates peak detection, making the case of d_1 = 3.2 µm the preferred choice for the subsequent analysis step.

The impact of varying silver-layer thicknesses (T_{Ag}) on sensor performance has also been explored, as depicted in Figure 3b. A rise in TAg results in a blue-shift of confinement loss, accompanied by a decrease in corresponding intensity. This trend is attributed to the fact that a thinner silver medium induces more interaction of light-matter, leading to enhanced oscillation of SP. This

phenomenon amplifies the decaying field near the interface. Consequently, we consider T_{Ag} = 20 nm the optimal thickness for the next simulation.

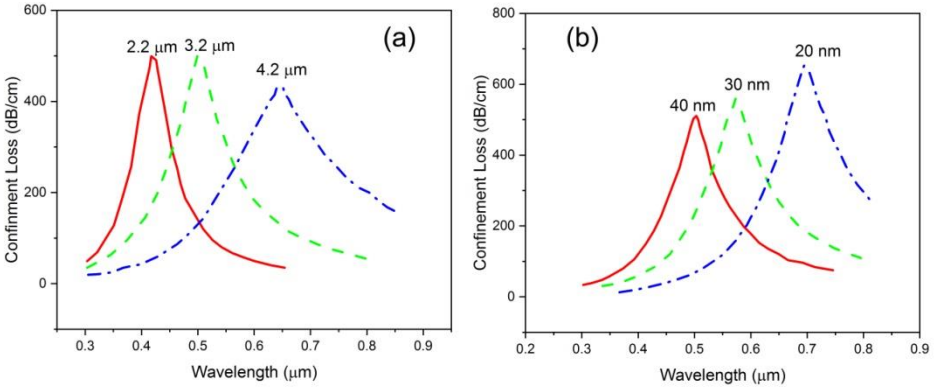

Fig. 3. (a) Evolution of confinement loss for various d_1 values. (b) Fluctuation of core mode confinement loss for different T_{Ag} values.

We have also explored how changing lattice pitch lengths affects the confinement loss parameter. Fig. 4a illustrates the computed confinement loss when the pitch value is changed. It is evident that as Λ increases, the loss peak is blue-shifted while its amplitude amplifies. This behavior can be attributed to the fact that larger Λ values cause the core's light to penetrate into the cladding, consequently boosting the decaying electromagnetic field and resulting in increased loss. As it can be seen the resonance peak is shifted which is associated with the change of detected analyte's RI. With a consistent loss distribution and a peak observed within the analyzed band, our sensor proves to be a strong candidate for various sensing applications. In Fig. 4b, the confinement loss for diverse analyte refractive indices ranging in the range of 1.33~1.36 are depicted. Employing the wavelength-interrogation method, as the RI changes, the wavelength of resonance is adjusted from 0.5 ~ 0.7 μm. Results show an average wavelength peak change of approximately 77 nm, rendering an average wavelength sensitivity (S_n) of 7700 nm/RIU. Optimal sensitivity arises as the analyte RI shifts in the range of 1.33~1.36, reaching a maximum of 9400 nm/RIU, with the RI resolution at 6.49×10^{-6} RIU. Fig. 5a presents the amplitude sensitivity calculated through the Amplitude Interrogation Method (AIM) for distinct analyte RIs. It is observed that the peak intensity diminishes as the RI fluctuates

in the range of 1.33~1.36, with the highest value reaching 215 RIU^{-1} while n_{Anl} equals 1.33.

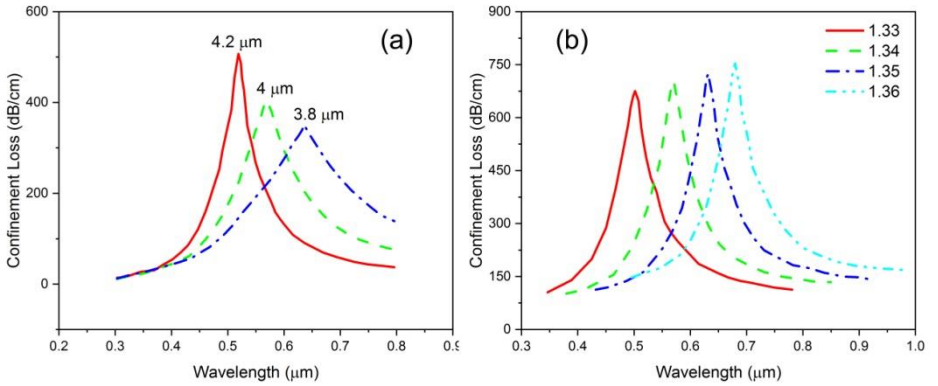

Fig. 4. (a) Evolution of core mode confinement loss across various lattice pitch Λ values. (b) Fluctuation of confinement loss for diverse analyte RI values.

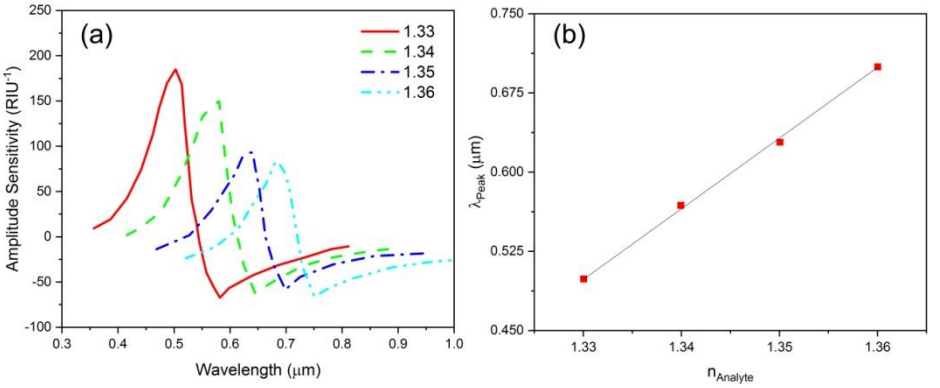

Fig. 5. (a) Computed amplitude sensitivity across varying analyte RIs. (b) Assessment of the degree of linearity between the analyte RI and resonance wavelength.

Finally, we conducted an analysis of the sensor's linearity by fitting the resonance wavelength values against analyte RIs, as illustrated in Fig. 5b

$$\lambda_{Peak} = 6.6 n_{Anl.} - 8.3 \quad (6)$$

The fitting equation yielded an adjusted coefficient of determination (R^2) of 0.99862, signifying a remarkably strong linear correlation between $n_{Anl.}$ and λ_{Peak}. In comparison to other structures (Table I), the proposed design and calculated sensitivity of the this sensor show it is a good candidate for many applications.

Table I. Comparison of properties: proposed sensor and reported ones.

Wavelength Sensitivity (nm/RIU)	Wavelength Resolution (RIU)	Amp. Sensitivity (RIU^{-1})	Ref.
2164	3.58×10^{-5}	376.76	[12]
2000	5×10^{-5}	200	[13]
2459	4.17×10^{-5}	-	[14]
9500	6.5×10^{-6}	215	This work

4. CONCLUSION

In summary, we conducted a numerical analysis of an efficient D-shaped PCF-SPR refractive index sensor in visible range. By considering a metal layer in the structure and optimized physical parameters, acceptable values of sensor performance is observed. The FEM was employed to thoroughly explore its characteristics. We investigated impact of structural parameters and examined the correlation of analyte refractive index and resonance wavelengths. Employing the wavelength interrogation method, we achieved an average 7700(nm/RIU) wavelength sensitivity and an average 1.08×10^{-5} *RIU* resolution. For analyte refractive indices in the range of 1.33~1.36, maximum wavelength sensitivity of 9400 nm/RIU and RI resolution of 6.49×10^{-6} RIU were obtained. Morover, calculations demonstrated an amplitude sensitivity of 215 RIU^{-1} for thr analyte refractive index of $n_{Anl.}$=1.33.

REFERENCES

[1] G. An, X. Hao, S. Li, X. Zhang. *D-Shaped Photonic Crystal Fiber Refractive Index Sensor Based on Surface Plasmon Resonance.* Appl. Opt. [Online]. 56 (24) (2017, Aug.) 6988-6922. Available: https://doi.org/10.1364/AO.56.006988

[2] J. J. Wu, S. Li, X. Wang, M. Shi, X. Feng, Y. Liu. *Ultrahigh Sensitivity Refractive Index Sensor of a D-Shaped PCF Based on Surface Plasmon Resonance*. Appl. Opt. [Online]. 57(15) (2018, May). 4002-4007. Available: https://doi.org/10.1364/AO.57.004002

[3] Z. Salehnezhad, M. Soroosh, A. Farmani. *Design and Numerical Simulation of a Sensetive Plasmonic-Based Nanosensor Utilizing MoS_2 Monolayer and Graphene*. DRM. [Online]. 131 (2023, Jan.) 109549. Available: https://doi.org/10.1016/j.diamond.2022.109594

[4] M. R. J. Azizpour, M. Soroush, N. Dalvand, Y. S. Kavian. *All-Optical Ultra-Fast Graphene-Photonic Crystal Switch*. Crystals. [Online]. 9 (2019, Sep.) 461. Available: https://doi.org/10.3390/cryst9090461

[5] M. Abbasi, M. Soroosh, E. Namjoo. *Polarization-Insensitive Temperature Sensor Based on Liquid Filled Photonic Crystal Fiber*. OPTIK. [Online]. 168 (2018, Sep.) 342-347. Available: https://doi.org/10.1016/j.ijleo.2018.04.116

[6] M. Tian, P. Lu, L. Chen, C. Lv, D. Liu. *All–solid D–shaped photonic fiber sensor based on surface plasmon resonance*. Opt. Commun. [Online]. 285 (2012, March) 1550–1554. Available: https://www.sciencedirect.com/science/article/abs/pii/S0030401811013447

[7] C. Ren, J. Yuan, K. Wang, B. Yan, X. Sang, C. Yu. *Design of Photonic Crystal Fiber Refractive Index Sensor Based on Surface Plasmon Resonance Effect for the Dual-Wavebands Measurement*. [Online]. Fiber. Integr. Opt. 40 (2020, Oct.) 263-275. Available: https://www.tandfonline.com/doi/full/10.1080/01468030.2020.1830204

[8] J. Wu, S. Li, X. Wang, M. Shi, X. Feng, Y. Liu. *Ultrahigh sensitivity refractive index sensor of a D–shaped PCF based on surface plasmon resonance*. [Online]. Appl. Opt. 57 (2018, May) 4002–4007. Available: https://opg.optica.org/ao/abstract.cfm?uri=ao-57-15-4002

[9] R. M. Osgood, N. C. Panoiu, J. I. Dadap, X. Liu, X. Chen, I. Hsieh, E. Dulkeith, W. M. J. Green, Y. A. Vlasov. *Engineering nonlinearities in nanoscale optical systems: Physics and applications in dispersion–engineered silicon nanophotonic wires.* [Online]. Adv. Opt. Photonics, 1 (2009, Jan.) 162–235. Available: https://opg.optica.org/aop/fulltext.cfm?uri=aop-1-1-162&id=176228

[10] J. N. Dash, R. Jha. *On the performance of graphene–based D–shaped photonic crystal fiber biosensor using surface plasmon resonance*. [Online]. Plasmonics, 10(5) (2015, Feb.) 1123–1131. Available: https://link.springer.com/article/10.1007/s11468-015-9912-7

[11] Y. Zhang, L. Xia, C. Zhou, X. Yu, H. Liu, D. Liu, Y. Zhang. Microstructured *fiber based plasmonic index sensor with optimized accuracy and calibration relation in large dynamic range*. [Online]. Opt. Commun. 284 (2011, Nov.) 4161–4166. Available: https://opg.optica.org/oe/fulltext.cfm?uri=oe-19-23-22863&id=224014

[12] H. Wu, Y. Song, M. Sun, Q. Wang. *Simulation of High-Performance Surface Plasmon Resonance Sensor Based on D-Shaped Dual Channel Photonic Crystal Fiber for Temperature Sensing*. [Online]. Materials. 16 (2022, Dec.) 37. Available: https://doi.org/10.3390/ma16010037

[13] S. Nivedha, P. R. Babu. K. Senthilnathan, *D-Shaped Plasmonic Sensor Using a Molybdenum Disulfide Doped Photonic Crystal Fiber*. [Online]. *IOP Conf. Ser. Mater. Sci. Eng.* 263 (2017) 5203. Available: http://doi.org/10.1088/1757-899X/263/5/052031

[14] H. Wang, H. Zhang, J. Dong, S. Hu, W. Zhu, W. Qiu, H. Lu, J. Yu, H. Guan, S. Gao. *Sensitivity-Enhanced Surface Plasmon Resonance Sensor Utilizing a Tungsten Disulfide (WS2) Nanosheets Overlayer*. [Online]. *Photon. Res.* 6 (2018) 485–491. Available: https://opg.optica.org/prj/abstract.cfm?uri=prj-6-6-485

[15] Momeni, M., Javadian Sarraf, M., Khatib, F. Design of high sensitivity and high FoM refractive index biosensor based on 2D-photonic crystal. *Journal of Optoelectronical Nanostructures*, 2021; 6(4): 33-58. doi: 10.30495/jopn.2022.27033.121720.1001.1.24237361.2021.6.4.3.1

[16] Heidary Orojloo, M., Jabbari, M., Solookinejad, G., Sohrabi, F. Design and modeling of photonic crystal Absorber by using Gold and graphene films. *Journal of Optoelectronical Nanostructures*, 2022; 7(2): 1-10. doi: 10.30495/jopn.2022.28915.123520.1001.1.24237361.2022.7.2.1.2

[17] Bazargani, M., Gharekhanlou, B., Banihashemin, M. Investigating the Design and Simulation of a Tunable Optical Filter Based on Photonic Crystal Using Selective Optofluidic Infiltration. *Journal of Optoelectronical Nanostructures*, 2022; 7(4): 66-79.

doi: 10.30495/jopn.2022.29582.1248

[18] Pathak, A.K., Singh, V.K.: SPR based optical fiber refractive index sensor using silver nanowire assisted CSMFC. IEEE Photonics Technol. Lett. 32(8), 465–468 (2020)

https://opg.optica.org/aop/fulltext.cfm?uri=aop-1-1-162&id=176228

[19] Pathak AK, Viphavakit C, Rahman BM, Singh VK. A highly sensitive SPR refractive index sensor based on microfluidic channel assisted with graphene-Ag composite nanowire. IEEE Photonics Journal. 2021 Mar 29;13(2):1-8.

https://www.tandfonline.com/doi/full/10.1080/01468030.2020.1830204

[20] Qiu, S., Chen, Y., Xu, F., Lu, Y.: Temperature sensor based on an isopropanol–sealed photonic crystal fiber in–line interferometer with enhanced refractive index sensitivity. Opt. Lett. 37, 863–865 (2012)

https://doi.org/10.1016/j.ijleo.2018.04.116

[21] Qiu SJ, Chen Y, Xu F, Lu YQ. Temperature sensor based on an isopropanol-sealed photonic crystal fiber in-line interferometer withenhanced refractive index sensitivity. Optics letters. 2012 Mar 1;37(5):863-5.

doi: 10.30495/jopn.2022.29582.1248

[22] Y. Okuno, Y. Saito, S. Kawata, P. Verma. Tip-enhanced Raman investigation of extremely localized semiconductor-to-metal transition of a carbon nanotube. Phys. Rev. Lett. 111, (2013) 216101. Available:10.1103/PhysRevLett.111.216101

[23] Shahi, S. Flattening Few Mode Fiber Laser Source Based on PMF and Loop Mirror in a Ring Cavity Resonator. *Journal of Optoelectronical Nanostructures*, 2023; 8(1): 84-94.

doi: 10.30495/jopn.2023.31308.1276

[24] Rifat, A.A., Ahmed, R., Yetisen, A.K., Butt, H., Sabouri, A., Mahdiraji, G.A., Yun, S.H., Adikan, F.M.: Photonic crystal fiber based plasmonic sensors. Sens. Actuat B Chem. 243, 311–325 (2017)

https://opg.optica.org/aop/fulltext.cfm?uri=aop-1-1-162&id=176228

[25] N. Lee, R. D. Hartschuh, D. Mehtani, A. Kisliuk, J. F. Maguire, M. Green, M. D. Foster, A. P. Sokolov, High contrast scanning nano-Raman spectroscopy of silicon. J. Raman Spectrosc. 38, (2007) 789–796.

Available:10.1002/jrs.1698